ACS APPLIED MATERIALS & INTERFACES

Research Article

www.acsami.org

Movable Magnetic Porous Cores Enclosed within Carbon Microcapsules: Structure-Controlled Synthesis and Promoted Carbon-Based Applications

Lijun You,[†] Yuting Zhang,[†] Shuai Xu, Jia Guo,* and Changchun Wang

State Key Laboratory of Molecular Engineering of Polymers, Department of Macromolecular Science, Fudan University, Shanghai 200433, P. R. China

Supporting Information

ABSTRACT: Rattle-type porous carbon microcapsules (RPCMs) were deliberately designed to combine multiple functions with the aim of improving the applicability of amorphous carbon in a synergistic fashion. A movable Fe_3O_4 nanocluster coated with porous carbon is encapsulated in the cavity of a carbon microcapsule with an eggshell-like characteristic, allowing for storage, adsorption, and exchange of matters through the mesoporous channels of the carbon layer. The synthetic strategy of RPCMs is flexible and universal, involving the constitution and carbonization of Fe_3O_4@PF@PS@PF template particles. This results in a double carbon shell and a sandwiched hollow cavity with a movable magnetic core. There is evidence that RPCMs possess large surface areas, hierarchical pore sizes, hydrophobicity, and magnetic responsiveness. Hence, diverse applications have been investigated. It is proved that RPCMs exhibit excellent performance in the effective enrichment of peptides/proteins. The detection limit toward peptides could reach as low as 10 nM, and the enrichment capacity toward MYO protein is as high as 410 mg/g (protein/beads). Furthermore, RPCMs are able to harvest proteins in complex real samples such as fetal bovine serum and rabbit blood. In addition, RPCMs could be fabricated in a supercapacitor electrode and display outstanding energy-storage performance. The electrochemical measurements demonstrate that RPCM-based electrodes have a specific capacitance of as high as 216 F/g (0.1 A/g), long-term cycling stability with a capacitance retention of 92.4% over 1000 cycles (0.2 A/g), and good electronic conductivity.

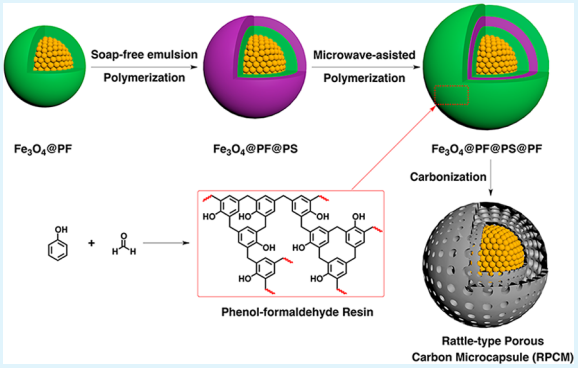

KEYWORDS: *magnetic nanoparticles, peptides/proteins enrichment, porous carbon, rattle structure, supercapacitor*

1. INTRODUCTION

Over the past decade, inorganic mesoporous materials have gained increasing research interest for their potential applications including catalysis,[1,2] host−guest chemistry,[3,4] adsorption,[5,6] and biomedical fields.[7,8] Mesoporous carbon materials, a pivotal branch of mesoporous materials, are highly appealing because of their controllable pore architecture, high surface area, large pore volume, electrical conductivity, and hydrophobic affinity. These features contribute to their excellent performance in various fields such as catalyst supports,[9,10] energy storage/conversion,[11,12] adsorbents,[13,14] and peptides/proteins enrichment.[15,16] In light of those distinctive advantages, "upgrade" of mesoporous carbon has been continuously acquired for crucial demand. In this context, the introduction of magnetic nanomaterials provides a high possibility of equipping mesoporous carbon with magnetic separation, catalytic activity, and conductivity. Thus, the design of magnetic mesoporous carbon composites will achieve the purpose of developing carbon-based materials for versatile applications.

To date, there are various strategies for the preparation of magnetic mesoporous carbon materials.[17−22] Following a conventional route, mesopores of carbon were charged with ferrofluids or iron salts for the subsequent in situ preparation of magnetic nanoparticles.[17,18] However, this method leads to a dramatic decrease of surface areas and a weak magnetic response. To tackle the issue, a nanocasting technique has been developed,[19] wherein magnetic mesoporous silica microspheres were synthesized as a hard template, and the carbon precursor infiltrated mesopores followed by the carbonization and removal of silica templates. However, the formed mesoporous carbon layers partially collapse upon elimination of the silica templates. The yields of products are thus not high, and the surface areas are also unsatisfactory. Along this line, rattle-type carbon microcapsules[23−25] with magnetic cores, a sandwiched hollow cavity, and porous shells have been designed and have immediately attracted considerable interest owing to high

Received: May 30, 2014
Accepted: August 12, 2014
Published: August 12, 2014

dx.doi.org/10.1021/am503421z | ACS Appl. Mater. Interfaces 2014, 6, 15179−15187

surface areas, large pore volumes, and superior performance in the storage and separation of guest molecules. However, the known preparation technique for the rattle-type magnetic mesoporous carbon microcapsules is too complicated and time-consuming. There are six steps involved in the process: (1) the magnetic core was prepared and (2) covered by nonporous SiO_2; (3) mesoporous SiO_2 was successively formed, resulting in a core−double-shell template particle; (4) the carbon precursor infiltrated the outer porous silica shell and was subjected to (5) high-temperature carbonization and (6) alkali etching of silica.[23,24] Therefore, the yield is low, and the silica-mediated pathway is not suited to large-scale production.

In this work, we propose a novel approach to the synthesis of rattle-type magnetic carbon microcapsules consisting of a movable Fe_3O_4 core and a double carbon shell. The well-defined structure is of many distinctive characteristics combining high surface areas, large pore volumes, appropriate mesopore sizes, hydrophobicity, magnetic responsiveness, and electronic storage and conduction. Hence, they promise great potential in a wide range of applications. More importantly, compared to the reported methods, our strategy is more attractive. Instead of silica, polystyrene (PS) is used as the sacrifice template to encapsulate magnetic cores and could be pyrolyzed to form a hollow cavity. Phenol−formaldehyde (PF) resin is used as the carbon source to afford a high carbon-forming yield. In addition, alternative constitution of PS and PF layers outside the core is possible to create a vesicle with multiple porous carbon shells and an isolated inner space. It is unprecedented and could not be implemented using the silica-mediated procedure.

To our knowledge, carbon-based materials are of significance in use for peptides/proteins adsorption[26,27] and electrode fabrication.[28−30] Endogenous peptides in serum contain much biological information, and the abundance is very low. Although mass spectrometry (MS) is a powerful tool for high-throughput analysis of peptides, MS analysis does not easily detect extremely low abundant peptides and is vulnerable to salts. Therefore, it is essential to enrich peptides and desalt protein digests prior to MS analysis by virtue of the hydrophobic properties of carbon-based materials. Herein, we proved the excellent and specific utility of rattle-type magnetic porous carbon microcapsules for hydrophobic enrichment of peptides/proteins. The enrichment capacity toward MYO protein could reach as high as 410 mg of proteins/g of beads. In addition, in view of long cycle life and high specific capacitance of carbon materials, we also validated that the combination of Fe_3O_4 and high-surface-area carbon could synergistically enhance the electrochemical performance, and the structural stability of capacitive electrodes was largely improved.

2. EXPERIMENTAL SECTION

2.1. Materials. Ferric chloride hexahydrate ($FeCl_3·6H_2O$), sodium acetate (NaOAc), ethylene glycol, trisodium citrate dehydrate (Na_3Cit), phenol, ammonia solution (25%), and formaldehyde solution (37%) were purchased from Shanghai Chemical Reagents Company. Styrene and 3-(trimethoxysilyl)propyl methacrylate were purchased from Sigma-Aldrich. Styrene was distilled under reduced pressure before use. Potassium persulfate (KPS) was purchased from Shanghai Aijian Reagent Company and recrystallized from water before use. Cytochrome *c* (Cyt *c*, 95%), myoglobin (MYO, 95%), horseradish peroxidase (HRP; 98%), ribonuclease B (RNB; 95%), and bovine serum albumin (BSA; 95%) were purchased from Sigma-Aldrich. Fetal bovine serum (FBS) and rabbit blood were supplied by Shanghai Ruijin Hospital. Deionized water was used in all experiments.

2.2. Preparation of Fe_3O_4@PF@PS@PF Microspheres. Carboxylate-stabilized Fe_3O_4 nanoclusters were solvothermally synthesized using our early method. Core−shell Fe_3O_4@PF microspheres were prepared by in situ polymerization of phenol and formaldehyde on Fe_3O_4 nanoclusters via the microwave-assisted hydrothermal approach.[31]

Fe_3O_4@PF@PS microspheres were synthesized by coating PS on Fe_3O_4@PF microspheres using a soap-free emulsion polymerization.[32] Typically, a 0.8 mg/mL Fe_3O_4@PF aqueous dispersion (125 mL) was prepared and bubbled with N_2 for 30 min. A total of 2.5 mL of styrene was added, and the mixture was heated to 70 °C. The reaction proceeded for 8 h after 80 mg of KPS was added to initiate the polymerization. After reaction, the product was collected by a magnet and thoroughly washed with water and ethanol.

Fe_3O_4@PF@PS microspheres were wrapped with PF by the microwave-aided hydrothermal method. The reaction was conducted on a CEM Discover microwave machine with single mode and continuous power at 2.45 GHz. In a typical procedure, 10 mg of Fe_3O_4@PF@PS microspheres was dispersed in the aqueous solution (30 mL) containing 40 mg of phenol, 0.2 mL of formaldehyde solution (37%), and 0.15 mL of ammonia (25%). The mixture was sonicated for 5 min to homogenize the dispersion. Then it was transferred into a microwave vessel with a holder. The desired temperature and time were programmed by the intelligent software before the reaction. The maximum power was set as 200 W, and the pressure limit was 180 psi. The reaction temperature was kept at 160 °C for 30 min. After the reaction was completed, the mixture was cooled to room temperature. The as-prepared microspheres were collected by a magnet and washed with water and ethanol three times, respectively, and dried under vacuum at 45 °C for 4 h. For the synthesis of carbon, PF particles were prepared using the same microwave-assisted hydrothermal conditions without the addition of any template particles. For the synthesis of single-carbon-layer RPCMs, Fe_3O_4@PS template particles were prepared by soap-free emulsion polymerization, and then they were coated by PF with the microwave-assisted method to result in Fe_3O_4@PS@PF template particles.

2.3. Preparation of Rattle-Type Porous Carbon Microcapsules (RPCMs). The Fe_3O_4@PF@PS@PF powders were heated to 650 °C at 10 °C/min under a N_2 flow, and carbonization was allowed to proceed for 2 h. The double carbon shell was formed, accompanied with decomposition of the sandwiched PS. The resulting microcapsules were washed with water and ethanol and dried under vacuum at 45 °C for 4 h. For comparison, the single-carbon-layer RPCMs and porous carbon were fabricated by carbonization of Fe_3O_4@PS@PF and PF particles, respectively.

2.4. Enrichment of Low-Abundant Peptides Using RPCMs. One mg/mL BSA in a NH_4HCO_3 buffer (pH 8.0, 25 mM) was digested with 1:40 trypsin/protein (w/w) for 12 h at 37 °C to produce tryptic digests of BSA. An aqueous dispersion of RPCMs (10 mg/mL) was prepared. To enrich peptides from a diluted solution, 2.0 μL of the RPCM dispersion (10 mg/mL) was added to a 50 mM ABC solution (100 μL) containing 10 nM BSA digests, and the mixture was sonicated at room temperature for 1 min. After the supernate was decanted with the help of a magnet, the RPCM with adsorbed peptides was washed three times with water to remove the salts of ABC. Then the peptides adsorbed within the RPCM were eluted with 5 μL of an eluent solution [80% acetonitrile (ACN) aqueous solution containing 5% trifluoroacetic acid (TFA)] for matrix-assisted laser desorption/ionization time-of-flight mass spectrometry (MALDI-TOF MS) analysis.

2.5. Enrichment of Proteins Using RPCMs. RPCM powders were washed with ethanol and then dispersed in water (20 mg/mL). A mixture of 5 μg of Cyt *c*, 5 μg of MYO, 5 μg of RNB, 5 μg of HRP, and 5 μg of BSA was dissolved in 100 μL of water containing 7 M urea and 2 M thiourea. Then 0.1 mg of RPCM was added, and the mixture was incubated at room temperature for 5 min with shaking. The protein-captured RPCM was washed twice by water with the assistance of a magnet. Then the stock, supernate, and RPCM with adsorbed proteins were lyophilized and used for sodium dodecyl sulfate−polyacrylamide gel electrophoresis (SDS-PAGE). For removal of proteins from the

Scheme 1. Synthetic Procedure of a RPCM

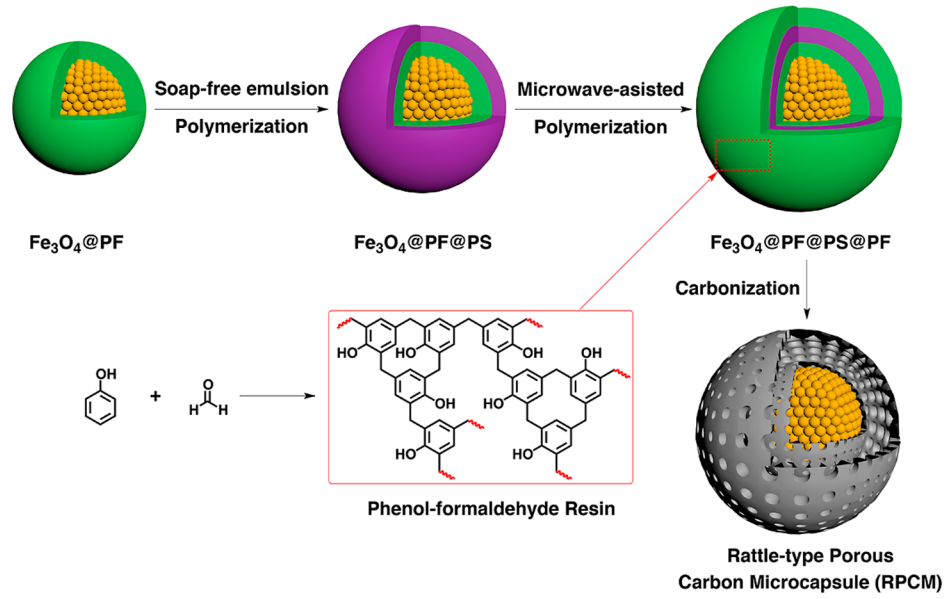

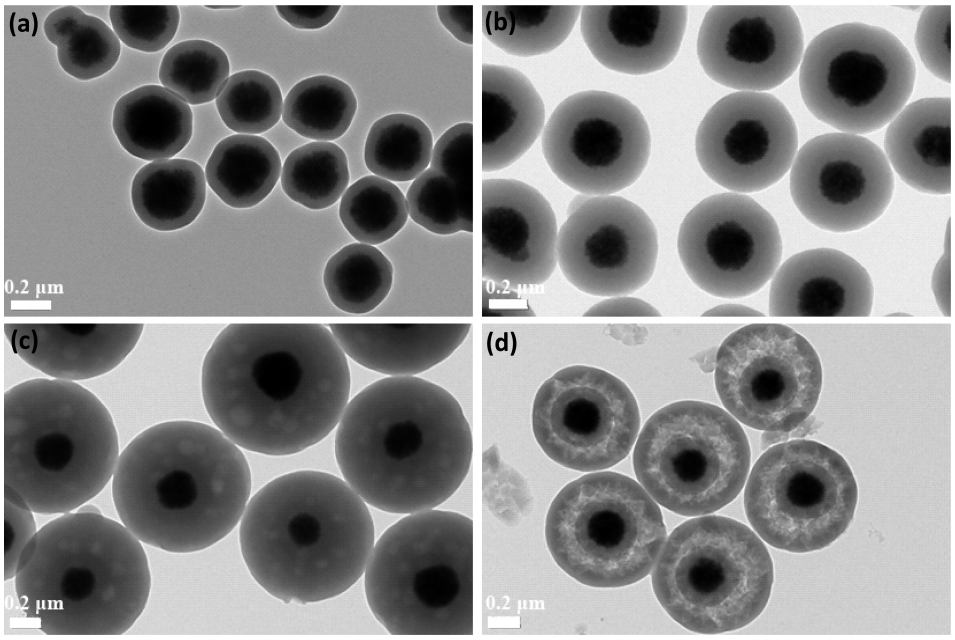

Figure 1. TEM images of Fe_3O_4@PF (a), Fe_3O_4@PF@PS (b), and Fe_3O_4@PF@PS@PF (c) microspheres and RPCMs (d).

real samples, FBS (1 μL) or rabbit blood (1 μL) was dissolved in 100 μL of water containing 7 M urea and 2 M thiourea. Then the same procedure was followed for analysis using SDS-PAGE.

2.6. Preparation of the Electrodes and Evaluation of the Electrochemical Properties. To evaluate the electrochemical properties of RPCM, the working electrodes were fabricated according to the following steps. RPCM, carbon black, and poly(vinylidene fluoride) were mixed in a weight ratio of 8:1:1, and isopropyl alcohol was used to yield a paste. The paste was pressed on a platinum mesh and dried in a vacuum oven at 40 °C overnight. The mass of active materials in the working electrode was 10 mg. A beaker-type three-electrode cell was equipped with a RPCM/platinum mesh working electrode, an Hg/Hg_2Cl_2 reference electrode, and a platinum flat counter electrode. For all electrochemical measurements, 1 M NaOH was used as the electrolyte. Cyclic voltammetry (CV), galvanostatic (GV) charge−discharge cycles, and electrochemical impedance spectroscopy (EIS) were conducted at room temperature. EIS measurements were carried out by applying an alternating-current voltage of 5 mV amplitude in the frequency range of 100 kHz to 10 mHz. The specific capacitance of the electrode is obtained from the following equation:

$$C_g = \frac{I\Delta t}{m\Delta V} \quad (1)$$

where C_g is the specific gravimetric capacitance (F/g), I is the loaded current (A), Δt is the discharge time (s), ΔV is the potential change during the discharge process (V), and m represents the mass of activated materials (g).

2.7. Characterizations. Transmission electron microscopy (TEM) images were taken on a JEM-2100F transmission electron microscope at an accelerating voltage of 200 kV. Samples dispersed at an appropriate concentration were cast onto a carbon-coated copper grid. Fourier transform infrared (FT IR) spectra were determined on a NEXUS-470 FT IR spectrometer, and the spectra were scanned over

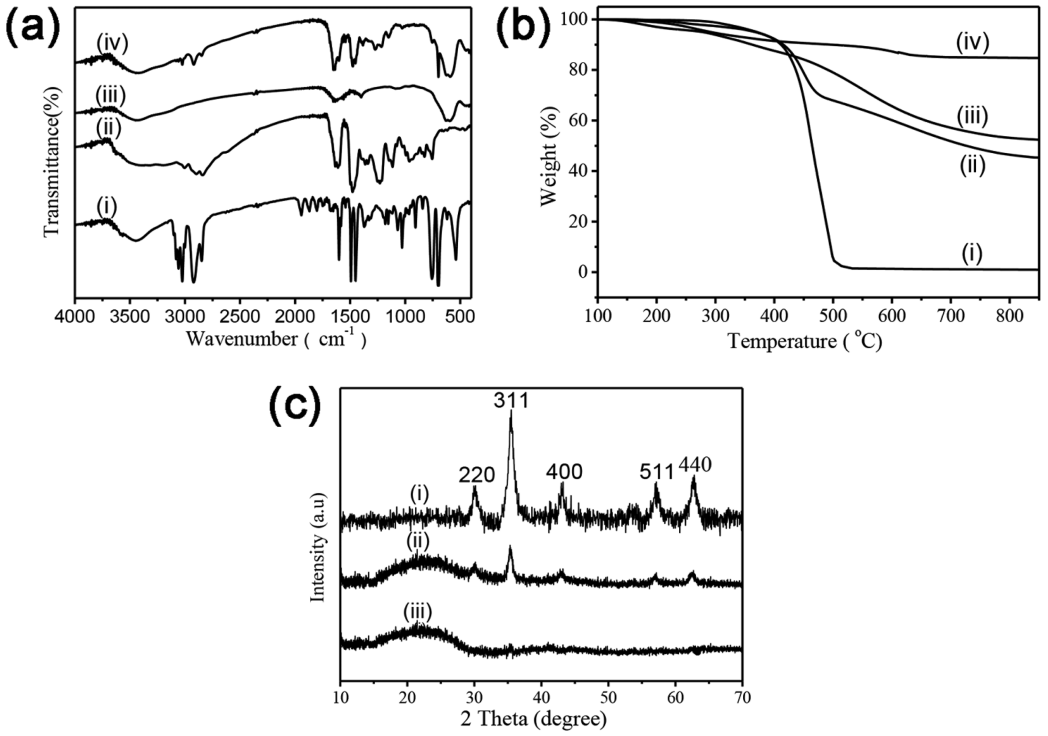

Figure 2. (a) FT IR spectra of PS (i), PF (ii), Fe_3O_4 (iii), and Fe_3O_4@PF@PS@PF microspheres (iv). (b) TGA curves of PS (i), Fe_3O_4@PF@PS@PF microspheres (ii), PF (iii), and Fe_3O_4 (iv). (c) PXRD patterns of Fe_3O_4 (i), RPCM (ii), and carbon (iii).

the range of 400−4000 cm^{-1}. All of the dried samples were mixed with KBr and then compressed to pellets. Thermogravimetric analysis (TGA) measurements were performed on a Pyris 1 TGA instrument from 100 to 800 °C under a constant N_2 flow of 40 mL/min. Powder X-ray diffraction (PXRD) patterns were collected on a X-ray diffraction spectrometer (Bruker D8 Advance, Germany) with Cu Kα radiation at λ = 0.154 nm operating at 40 kV and 40 mA. Magnetic characterizations were carried out by vibrating sample magnetometry (VSM) on a model 6000 physical property measurement system (Quantum Corp., San Jose, CA) at 300 K. CV, GV charge−discharge cycles, and EIS were conducted on a CHI 660A electrochemical workstation at room temperature. SDS-PAGE was performed using 4−15% precast polyacrylamide gels and a Mini-Protean Tetra cell (Tanon, China). Protein concentrations were obtained by measuring the absorbance at 413 nm using a BioTek Power Wave XS2 microplate reader. MALDI-TOF MS measurement was performed in the positive reflection mode on a 5800 Proteomic Analyzer (Applied Biosystems, Framingham, MA) with a Nd:YAG laser at 355 nm, a repetition rate of 400 Hz, and an acceleration voltage of 20 kV. Before measurement, 1 μL of an eluent solution was deposited on the plate and dried naturally, and then 0.5 μL of a CHCA matrix solution (5 mg/mL, 50% ACN aqueous solution containing 0.1% TFA) was dropped onto the sample-containing well. The range of laser energy was optimized to obtain good resolution and signal-to-noise ratio (S/N) and kept constant for further analysis. External mass calibration was performed using standard peptides from MYO digests.

3. RESULTS AND DISCUSSION

3.1. Synthesis of the RPCM. The synthesis procedure of the designed RPCM is illustrated in Scheme 1. The Fe_3O_4@phenol-formaldehyde-resin (Fe_3O_4@PF) microspheres were prepared via the microwave-assisted hydrothermal method following our reported route.[31] A PS shell was coated on the Fe_3O_4@PF microspheres through a soap-free seeded emulsion polymerization. Again, PF was formed on Fe_3O_4@PF@PS microspheres, resulting in an alternative triple PF/PS/PF shell. The as-synthesized Fe_3O_4@PF@PS@PF microspheres were then subjected to carbonization at 650 °C under a N_2 flow. In this process, PF layers were converted to porous carbon, accompanied by thermolysis of the PS shell. Thus, the hollow space was sandwiched between the outer and inner porous carbon layers, as displayed in Scheme 1, and Fe_3O_4 nanoparticles covered by porous carbon are movable within microcapsules. The one-step approach to conversion of the template particles to rattle-type microcapsules is facile and efficient in control of the multilevel microstructure.

TEM images of Fe_3O_4-enclosed microspheres and microcapsules are shown in Figure 1. It can be seen that the assembled inorganic nanoparticles are encapsulated by a PF shell with an average thickness of 50 nm. With extension from one PF layer to a triple PF/PS/PF layer, the particle sizes were correspondingly increased from approximately 320 to 510 to 700 nm. It implies the efficient casting of PS and PF on each other, but they are difficult to distinguish in the TEM images. We roughly accessed the total thickness of PS and the second PF shells, up to ~90 nm. Upon carbonization, the PS layer decomposed to form the void sandwiched by the inner and outer carbon shells with sizes of 50 and 70 nm, respectively (Figure 1d). The decrease of the shell thickness may be attributed to the release of noncarbon components during the carbonization process.

To qualitatively confirm the coating of PS and PF shells on Fe_3O_4 nanoclusters, Fe_3O_4, PS, PF, and Fe_3O_4@PF@PS@PF microspheres were characterized by FT IR spectroscopy (Figure 2a). It can be seen that the PS spectrum gives characteristic bands of 3011−3091 cm^{-1} due to the C−H bond of benzene, 2845 and 2928 cm^{-1} due to the CH_2 groups of the PS chain, and 1600, 1378, and 538 cm^{-1} due to the substituted benzene ring.[33] For the spectrum of PF, the broad band at 3432 cm^{-1} corresponds to the stretching of −OH, the bands at 1600,1476, 822, and 753 cm^{-1} are the characteristic absorption

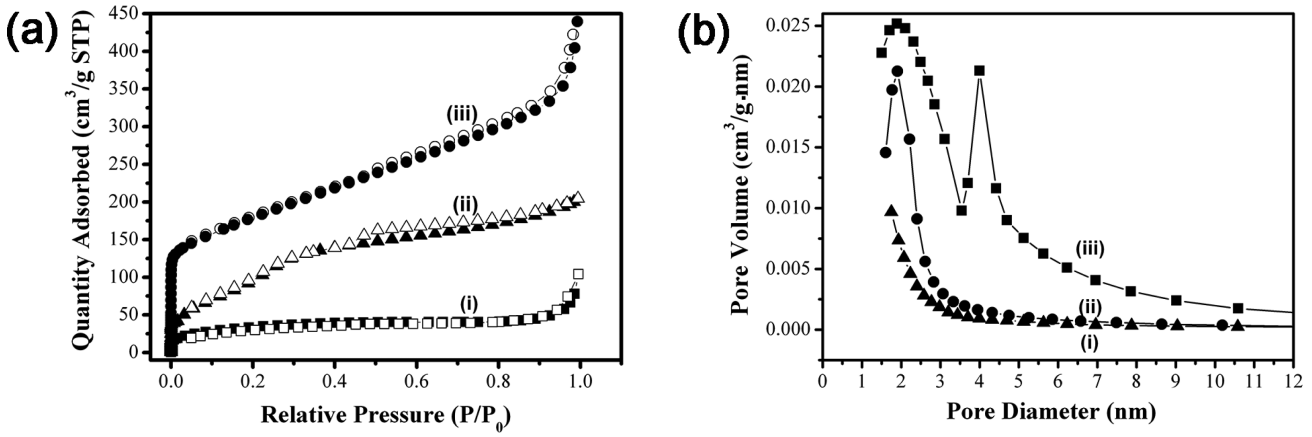

Figure 3. N_2 adsorption−desorption isotherms at 77 K (a) and pore-size distributions (b) of Fe_3O_4 (i), carbon (ii), and RPCM (iii).

of benzene rings,[34] the band at 1345 cm^{-1} is from the phenolic OH, and the bands at 1242 and 1111 cm^{-1} are from the C−O stretch. In the FT IR spectrum of Fe_3O_4 nanoclusters, the characteristic bands are found at 595 cm^{-1} ascribed to Fe−O bonds and at 1640 and 1401 cm^{-1} derived from vibrations of carboxylate groups of citrate used as a stabilizer for Fe_3O_4. Compared with the three reference spectra, the characteristic peaks of Fe_3O_4 (595 cm^{-1}), PF (1648, 1486, 1370, 1276, 1146, and 819 cm^{-1}), and PS (2845, 1593, and 691 cm^{-1}) could all be found in the spectrum of composite microspheres, implying the formed multicomponent structure.

The thermal stability and quantitative assessment of compositions were investigated by TGA under a N_2 atmosphere from 100 to 800 °C (Figure 2b). 10% weight loss for Fe_3O_4 nanoclusters was found as a result of thermolysis of a citrate stabilizer on the clusters. PS was completely decomposed near 500 °C, indicating that the hollow cavity of RPCMs could be formed with thermolysis of the PS shell (650 °C). There were two thermal degradation regions observed for PF. This can be explained by water removal during condensation and carbonization of PF.[35] With reference of Fe_3O_4, PF, and PS, the composite microspheres show the understandable degradation behavior. The first stage was in the range of 400−500 °C with 10% weight loss due to decomposition of PS, and the second stage above 500 °C showed a slow decline with 21% weight loss. It is possibly caused by partial pyrogenation and carbonization of the PF component.[35]

The magnetic hysteresis curves (Figure S1a in the SI) measured by VSM demonstrate that all of the microspheres have no obvious remanence and coercivity at 300 K. Compared to the saturation magnetization (M_s) of Fe_3O_4 (72.5 emu/g), the M_s value of RPCMs was reduced (11.9 emu/g), but they still could rapidly respond to an external magnetic field and are separated from the aqueous solution within 5 s (Figure S1b in the SI). Also, RPCMs are superparamagnetic, allowing for multiple cycles of enrichment/dispersion in the medium.

The crystalline structure and phase purity were determined by PXRD, as shown in Figure 2c. Fe_3O_4 and porous carbon were applied as references. The typical diffraction peaks of Fe_3O_4 crystals were all found in the PXRD pattern of the RPCM, indicating that the crystalline structure of Fe_3O_4 was well retained under solvothermal conditions. In addition, one can see a broad peak at $\theta = 22°$. This may be derived from the amorphous phase of the carbon component when referring to the diffraction pattern of carbon.

Figure 3 shows the N_2 adsorption−desorption isotherms and pore-size distributions of Fe_3O_4, carbon, and RPCMs, respectively. According to IUPAC classification, Fe_3O_4 nanocluster, carbon, and RPCMs all have type IV sorption isotherms, indicative of mesoporous character. Compared with the other two, RPCMs displayed a steep increase in adsorption at the low relative pressure region. This implies that the micropore is formed after carbonization of the PF component. The total pore volumes, average particle sizes, and surface areas are summarized in Table 1. Using the

Table 1. Porous Parameters of Fe_3O_4, Carbon, and RPCM

sample	S_{BET} (m^2/g)[a]	pore volume (cm^3/g)[b]	pore size (nm)[c]
Fe_3O_4	117	0.12	5.6
carbon	425	0.32	3.0
RPCM	622	0.68	4.9

[a]Calculated from the N_2 adsorption isotherm using the BET model. [b]Total pore volume at P/P_0 = 0.99. [c]Calculated from the N_2 desorption isotherm using the BJH model.

Brunauer−Emmett−Teller (BET) model, RPCMs show the highest surface area and pore volume, up to 622 m^2/g and 0.68 cm^3/g, respectively. We reason that the double-carbon-layer structure is beneficial to enhance the porosity of RPCMs. To prove it, the single-carbon-layer RPCM (Fe_3O_4@air@carbon) was synthesized by carbonization of the Fe_3O_4@PS@PF template particles. The well-defined rattle-type microstructure could be observed in the TEM image (Figure S2a in the SI). The N_2 sorption isotherm demonstrates that they are of equal mesoporosity, and the surface area and pore volume were calculated to be 314 m^2/g and 0.29 cm^3/g, respectively. The result elucidates that the increasing number of carbon layers could notably improve the surface areas and pore volumes. The pore-size distribution was evaluated using the Barrett−Joyner−Halenda (BJH) model (Figure 3b). RPCM shows a dual-pore-size distribution centered at 2.2 and 4.5 nm. Also, we found that the pore sizes of carbon and single-carbon-layer RPCMs were distributed at 2.2 and 4.0 nm (Figures 3b and 2Sb in the SI), respectively. Thus, it is most likely that the dual-pore-size distribution from RPCMs is derived from the differential carbon-layer structures. The dominated mesopores are large enough to accommodate biomacromolecules in selective

enrichment, and the hierarchical pore effect is conducive to storage charges for use in supercapacitance.[36]

3.2. Enrichment of Low-Abundant Peptides. Endogenous peptides play an important role in many biological processes,[15,27] while they are always expressed at extremely low abundance and are present in the buffer of high salt concentration. These issues are difficult to detect using MS analysis. Thus, enrichment of peptides prior to MALDI-TOF MS analysis is an essential step. It is well-known that carbon-based materials can adsorb low-abundant peptides/proteins by virtue of hydrophobic interaction. RPCMs not only combine hydrophobicity, high surface area, large pore volume, and magnetic responsiveness but also possess the hollow inner space to improve the adsorption efficiency.

With all this in mind, the enrichment efficiency of RPCM for peptides was evaluated. The dispersion of RPCMs was mixed with a solution of 50 mM ABC containing tryptic digests of BSA, and it was incubated for 1 min. After screening of enrichment conditions including the incubation time, elution time, and compositions of eluate, the optimized results could be obtained during the following process: a mixture of peptides and RPCM was ultrasonically dispersed for 1 min at room temperature; the elution of peptides was mixed with an eluate, a 80% ACN aqueous solution containing 5% TFA, and was sonicated for 5 min. Figure 4a shows the original solution of 10

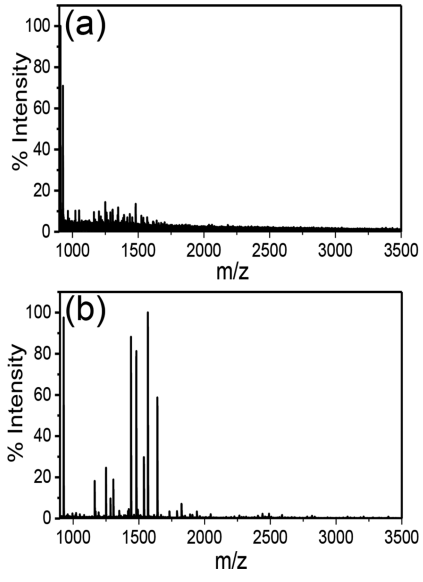

Figure 4. MALDI MS spectra of the tryptic digest of 10 nM BSA without (a) and with (b) enrichment using RPCM.

nM BSA digests detected by MALDI-TOF MS. The result proves that peptides at such a low concentration are hardly detected without the enrichment step. Upon harvesting of peptides with RPCM, the enhanced signals of BSA were explicitly observed. The S/N ratios of three distinct peptides were increased from 37 (m/z 1480.15), 41 (m/z 1568.12), and 65 (m/z 1640.34) to 10331, 12947, and 7540, respectively. Furthermore, when the concentration of the original BSA solution was decreased to 0.1 nM, some peaks were still found after enrichment. This demonstrates high sensitivity toward hydrophobic peptides (Figure S3 in the SI). Because the RPCM has appropriate mesopore channels and a large cavity, the enrichment could be rapidly completed in 1 min, outperforming the previous work, which usually spends at least 30 min to complete the enrichment.[24,26]

3.3. Enrichment of Proteins from Standard or Real Samples. To further elucidate the applicability of RPCMs in the enrichment of proteins, we attempted to validate whether the high hydrophobicity of carbon resulted in a strong retention of proteins on the adsorbent. To our knowledge, salts/buffers used in sample preparation may interfere with protein identification in subsequent MS analysis, especially for low-abundant proteins. Thus, enrichment is a matter of not only concentrating samples but also depleting these salts/buffers. Within the context, we prepared proteins in the solution of 7 M urea and 2 M thiourea, a commonly used buffer for protein extraction, to mimic biological samples. The enrichment results of RPCMs toward proteins are shown in Figure 5. Upon

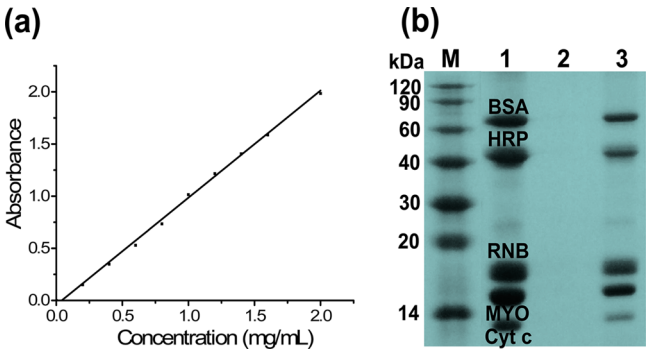

Figure 5. (a) Standard curve of the MYO concentration determined by UV−vis at 413 nm. (b) SDS-PAGE analysis of the enriched proteins. Lane M: protein molecular weight marker. Lane 1: mixed proteins before enrichment. Lane 2: supernate after enrichment with the RPCM. Lane 3: mixed proteins adsorbed by the RPCM.

treatment using RPCMs, all of the proteins were effectively separated and most of them could be released from the microcapsules under electrophoresis. We determined the binding capacity of RPCM toward MYO protein to be around 410 mg/g (protein/beads) measured by a microplate reader at a wavelength of 413 nm. This value is higher than the binding capacities of carbon without a hollow cavity (290 mg/g) and a single-carbon-layer RPCM (324 mg/g). Also, it is larger than most of the hydrophobic materials.[15,37] The adsorption and desorption properties of RPCMs toward MYO were studied (Figure S4 in the SI). One can see that the MYO release efficiency is approximately 50% when eluting with 10% SDS. The reason may lie in the fact that the extreme hydrophobicity and multilevel pore structure inhibit the protein release to some extent.

To investigate the practical use of RPCMs, FBS was selected as a real biological sample. In Figure 6a, the large amount of proteins from FBS could be effectively enriched and released from the microcapsules under electrophoresis. Despite big interferences such as carbohydrates, hormones, or fats, highly efficient enrichment was achieved, proving that the RPCM is an ideal tool for the desalting of real systems. Analogously, more intricate biological sample rabbit blood was utilized to evaluate the adsorption capacity. RPCM shows an outstanding enrichment/release performance toward target proteins. Therefore, in light of the ability to fish low-abundant peptides or desalt and concentrate proteins, RPCM is expected to promote the MS-aided proteomic analysis in real samples for early diagnosis and treatment.

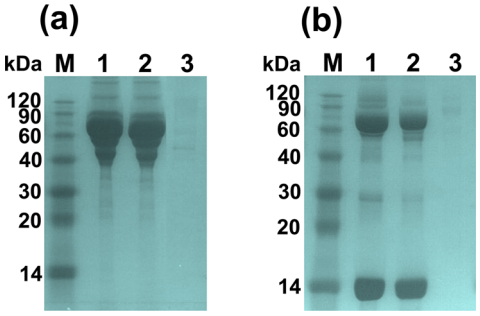

Figure 6. SDS-PAGE analysis of the proteins removed from FBS (a) and rabbit blood (b). Lane M: protein molecular weight marker. Lane 1: FBS or rabbit blood before enrichment. Lane 2: proteins released from the RPCM. Lane 3: supernate of FBS or rabbit blood after enrichment.

3.4. Electrochemical Performance. It has been reported that 2−8 nm pore sizes in the mesopore region are conducive to improving the power performance at high current densities and ion diffusion in electrodes. Also, micropores (<2 nm) are accessible to electrolyte ions for the promotion of energy storage.[36] Thus, the use of RPCMs as electrode materials is advantageous because their pore sizes are simultaneously populated in the regions of micropore and mesopore. To validate the structural advances of RPCMs, we conducted a series of electrochemical measurements for the RPCM-blending electrodes. Fe_3O_4, single-carbon-layer RPCM, and carbon were all used as controls for comparison. A three-electrode cell was prepared, and the CV curves were obtained at a voltage scan rate of 200 mV/s, as displayed in Figure 7a. The CV curve of Fe_3O_4 shows the redox peaks, indicative of their pseudocapacitive behavior. The rectangular CV curve of carbon reflects the character of double-layer capacitance. In comparison to Fe_3O_4 and carbon, two kinds of RPCMs give rectangular CV curves with larger enclosed areas. Calculated from the curves in Figure 7a, the CV integrated areas of Fe_3O_4, carbon, single-carbon-layer RPCM, and RPCM were 0.1018, 0.1440, 0.7993, and 1.361, respectively. The results suggest that RPCMs are desired in enhancement of the specific capacitance. With an increase in the scan rates from 5 to 200 mV/s (Figure S5 in the SI), the shapes of the CV curves were changed slightly, implying a small equivalent series resistance and weak polarization of the electrodes.[38]

The charge−discharge behavior of the electrodes was evaluated by the GV charge−discharge tests. As depicted in Figure 7b, RPCMs allow a much longer charge−discharge time than those of Fe_3O_4, carbon, and single-carbon-layer RPCM at a current density of 0.2 A/g. The charging curve is nearly symmetrical to the discharging counterpart, which corroborates the electrochemical reversibility of the RPCM-based electrode. The specific capacitance values of RPCMs, single-carbon-layer RPCMs, carbon, and Fe_3O_4 were calculated from the discharge curves as 181, 106, 90, and 11 F/g, respectively. Also, when the current density was varied from 0.1 to 0.4 to 1 A/g (Figure S6 in the SI), the specific capacitances of RPCM-based electrodes

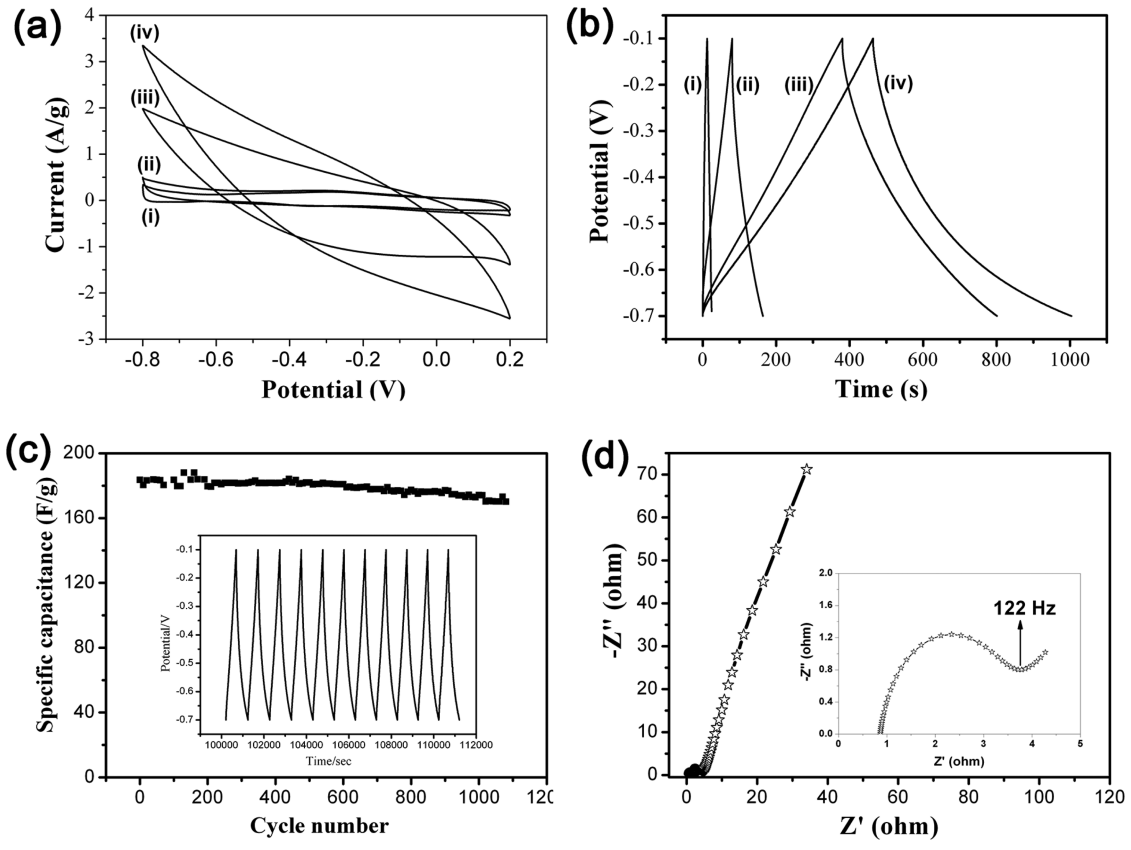

Figure 7. (a) CV curves of Fe_3O_4 (i), carbon (ii), single-carbon-layer RPCM (iii), and RPCM (iv) electrodes at a voltage scan rate of 200 mV/s. (b) GV charge−discharge curves of Fe_3O_4 (i), carbon (ii), single-carbon-layer RPCM (iii), and RPCM (iv) electrodes at a current density of 0.2 A/g. (c) Cycling performance test of the RPCM electrode (0.2 A/g). (d) Nyquist plot of the RPCM electrode. The inset of part c contains the GV charge−discharge curves of 11 cycles. The inset of part d is a magnified view of a plot in the high-frequency range.

dx.doi.org/10.1021/am503421z | ACS Appl. Mater. Interfaces 2014, 6, 15179−15187

retained a high level, up to 216, 148, and 126 F/g correspondingly. As far as we know, under the same current density (0.1 A/g), the capacitive performance of the RPCM electrode (216 g/F) pronouncedly surpasses that of other known iron oxide/carbon composite materials such as Fe_3O_4/ACN (37.9 F/g),[28] Fe_3O_4/MWNT (165 F/g),[39] Fe_2O_3/graphene (151.8 F/g),[40] and Fe_3O_4/CNF (135 F/g).[41] The reason is that the combination of a double carbon layer (attributed to electric double-layer capacitance) with Fe_3O_4 (attributed to pseudocapacitance), as well as large surface areas and multilevel pore sizes, is responsible for a synergistic effect to enhancement of the specific capacitance.

The long-term cycling stability of the RPCM electrode was examined by GV charge−discharge cycling techniques at a current density of 0.2 A/g (Figure 7c). Retention of the specific capacitance is as high as 92.4% of the initial capacitance after 1000 cycles. Meanwhile, a random examination of 11 charge−discharge cycles displays the reversible and symmetric curves (inset of Figure 7c). We reason that the inner cavity sandwiched between the carbon shells may allow for volume expansion and contraction so as to relax the strain stress of activated carbon, and thus the RPCM electrode could endure the numerous charging−discharging cycles while retaining its prominent structural stability.

To further survey the electrochemical performance of the RPCM electrode, EIS measurement was carried out, and the EIS data were expressed in the Nyquist plot in Figure 7d. An approximately 70° slope in the plot implies the effective storage of charges in electrodes.[28] Estimated from the intercept on the real axis in the high-frequency range, the solution resistance R_s was as low as 0.86 Ω, revealing the good electrical conductivity of the RPCM electrode. Also, the charge-transfer resistance R_{ct} was calculated as 3.84 Ω, showing the facile charge-transfer ability and high specific power density of the RPCM electrode.

4. CONCLUSIONS

Porous carbon microcapsules with rattle-type architecture were controllably synthesized through a microwave-assisted hydrothermal route and a one-step calcination process. The advantageous structures render RPCMs with large surface areas, hierarchical pore sizes, hydrophobic affinity, electrical conductivity, and magnetic responsiveness. Therefore, they exhibit excellent performances in the enrichment of peptides/proteins in standard samples and real complex samples and distinctive capacitive characteristics including high capability, reversibility, and long-term cycling stability. We believe that our findings will encourage further work in the exploration of carbon-based microcapsules for prospective broader applications.

■ ASSOCIATED CONTENT

Supporting Information

VSM curves, magnetic separation photographs, a MALDI MS spectrum, adsorption and desorption curves, a TEM image, N_2 sorption isotherms, CV curves, and GV charge−discharge curves. This material is available free of charge via the Internet at http://pubs.acs.org.

■ AUTHOR INFORMATION

Corresponding Author

*E-mail: guojia@fudan.edu.cn.

Author Contributions

†L.J.Y. and Y.T.Z. contributed equally.

Notes

The authors declare no competing financial interest.

■ ACKNOWLEDGMENTS

This work is supported by the NSFC (Grants 21004012 and 21128001), STCSM (Grants 13520720200 and 14ZR1402300), and the research fund of Key Laboratory for Advanced Technology in Environmental Protection of Jiangsu Province. We also thank Prof. Peng for measurement support on electrochemical characterization.

■ REFERENCES

(1) Corma, A. From Microporous to Mesoporous Molecular Sieve Materials and Their Use in Catalysis. *Chem. Rev.* **1997**, *97*, 2373−2419.

(2) Deng, Y. H.; Cai, Y.; Sun, Z. K.; Liu, J.; Liu, C.; Wei, J.; Li, W.; Liu, C.; Wang, Y.; Zhao, D. Y. Multifunctional Mesoporous Composite Microspheres with Well-Designed Nanostructure: A Highly Integrated Catalyst System. *J. Am. Chem. Soc.* **2010**, *132*, 8466−8473.

(3) Wang, Y. M.; Wu, Z. Y.; Wang, H. J.; Zhu, J. H. Fabrication of Metal Oxides Occluded in Ordered Mesoporous Hosts via a Solid-State Grinding Route: The Influence of Host−Guest Interactions. *Adv. Funct. Mater.* **2006**, *16*, 2374−2386.

(4) Ye, G.; Bai, F. F.; Chen, G. J.; Wei, J. C.; Wang, J. C.; Chen, J. A Novel Well-Ordered Mesoporous Organosilica Specialized for Highly Selective Recognition of Pb(II) by Host−Guest Interactions. *J. Mater. Chem.* **2012**, *22*, 20878−20880.

(5) Liu, S. S.; Chen, H. M.; Lu, X. H.; Deng, C. H.; Zhang, X. M.; Yang, P. Y. Facile Synthesis of Copper(II) Immobilized on Magnetic Mesoporous Silica Microspheres for Selective Enrichment of Peptides for Mass Spectrometry Analysis. *Angew. Chem., Int. Ed.* **2010**, *49*, 7557−7561.

(6) Zhang, Y. T.; Li, L. L.; Ma, W. F.; Zhang, Y.; Yu, M.; Guo, J.; Lu, H. J.; Wang, C. C. Two-in-One Strategy for Effective Enrichment of Phosphopeptides Using Magnetic Mesoporous γ-Fe_2O_3 Nanocrystal Clusters. *ACS Appl. Mater. Interfaces.* **2013**, *5*, 614−621.

(7) Gai, S. L.; Yang, P. P.; Li, C. X.; Wang, W. X.; Dai, Y. L.; Niu, N.; Lin, J. Synthesis of Magnetic, Up-Conversion Luminescent, and Mesoporous Core−Shell-Structured Nanocomposites as Drug Carriers. *Adv. Funct. Mater.* **2010**, *20*, 1166−1172.

(8) Luo, B.; Xu, S.; Luo, A.; Wang, W. R.; Wang, S. L.; Guo, J.; Lin, Y.; Zhao, D. Y.; Wang, C. C. Mesoporous Biocompatible and Acid-Degradable Magnetic Colloidal Nanocrystal Clusters with Sustainable Stability and High Hydrophobic Drug Loading Capacity. *ACS Nano* **2011**, *5*, 1428−1435.

(9) Zhang, Y. H.; Wang, A. Q.; Zhang, T. A New 3D Mesoporous Carbon Replicated from Commercial Silica as a Catalyst Support for Direct Conversion of Cellulose into Ethylene Glycol. *Chem. Commun.* **2010**, *46*, 862−864.

(10) Su, F. B.; Zeng, J. H.; Bao, X. Y.; Yu, Y. S.; Lee, J. Y.; Zhao, X. S. Preparation and Characterization of Highly Ordered Graphitic Mesoporous Carbon as a Pt Catalyst Support for Direct Methanol Fuel Cells. *Chem. Mater.* **2005**, *17*, 3960−3967.

(11) Wen, Z. H.; Li, J. H. Hierarchically Structured Carbon Nanocomposites as Electrode Materials for Electrochemical Energy Storage, Conversion and Biosensor Systems. *J. Mater. Chem.* **2009**, *19*, 8707−8713.

(12) Nishihara, H.; Kyotani, T. Templated Nanocarbons for Energy Storage. *Adv. Mater.* **2012**, *24*, 4473−4498.

(13) Zhuang, X.; Wan, Y.; Feng, C. M.; Shen, Y.; Zhao, D. Y. Highly Efficient Adsorption of Bulky Dye Molecules in Wastewater on Ordered Mesoporous Carbons. *Chem. Mater.* **2009**, *21*, 706−716.

(14) Zhang, Y. X.; Xu, S. C.; Luo, Y. Y.; Pan, S. S.; Ding, H. L.; Li, G. H. Synthesis of Mesoporous Carbon Capsules Encapsulated with

Magnetite Nanoparticles and Their Application in Wastewater Treatment. *J. Mater. Chem.* **2011**, *21*, 3664−3671.
(15) Qin, H. Q.; Gao, P.; Wang, F. J.; Zhao, L.; Zhu, J.; Wang, A. Q.; Zhang, T.; Wu, R. A.; Zou, H. F. Highly Efficient Extraction of Serum Peptides by Ordered Mesoporous Carbon. *Angew. Chem., Int. Ed.* **2011**, *50*, 12218−12221.
(16) Wu, Z. X.; Zhao, D. Y. Ordered Mesoporous Materials as Adsorbents. *Chem. Commun.* **2011**, *47*, 3332−3338.
(17) Fuertes, A. B.; Tartaj, P. Monodisperse Carbon−Polymer Mesoporous Spheres with Magnetic Functionality and Adjustable Pore-Size Distribution. *Small* **2007**, *3*, 275−279.
(18) Wang, Y. G.; Li, Bo.; Zhang, C. L.; Song, X. F.; Tao, H.; Kang, S. F.; Li, X. A Simple Solid−Liquid Grinding/Templating Route for the Synthesis of Magnetic Iron/Graphitic Mesoporous Carbon Composites. *Carbon* **2013**, *51*, 397−403.
(19) Guo, L. M.; Zeng, S. Z.; Li, J. T.; Cui, F. M.; Cui, X. Z.; Bu, W. B.; Shi, J. L. An Easy Co-Casting Method to Synthesize Mesostructured Carbon Composites with High Magnetic Separability and Acid Resistance. *New J. Chem.* **2009**, *33*, 1926−1931.
(20) Guo, L. M.; Cui, X. Z.; Li, Y. S.; He, Q. J.; Zhang, L. X.; Bu, W. B.; Shi, J. L. Hollow Mesoporous Carbon Spheres with Magnetic Cores and Their Performance as Separable Bilirubin Adsorbents. *Chem.—Asian J.* **2009**, *4*, 1480−1485.
(21) Liu, J.; Qiao, S. Z.; Hu, Q. H.; Lu, G. Q. Magnetic Nanocomposites with Mesoporous Structures: Synthesis and Applications. *Small* **2011**, *7*, 425−443.
(22) Zhai, Y. P.; Dou, Y. Q.; Liu, X. X.; Park, S. S.; Ha, C. S.; Zhao, D. Y. Soft-Template Synthesis of Ordered Mesoporous Carbon/Nanoparticle Nickel Composites with a High Surface Area. *Carbon* **2011**, *49*, 545−555.
(23) Zhang, X.; Jiang, L. Fabrication of Novel Rattle-type Magnetic Mesoporous Carbon Microspheres for Removal of Microcystins. *J. Mater. Chem.* **2011**, *21*, 10653−10657.
(24) Wan, H.; Qin, H. Q.; Xiong, Z. C.; Zhang, W. B.; Zou, H. F. Facile Synthesis of Yolk−Shell Magnetic Mesoporous Carbon Microspheres for Efficient Enrichment of Low Abundance Peptides. *Nanoscale* **2013**, *5*, 10936−10944.
(25) Yin, Y. Y.; Zhou, S. X.; Min, C.; Wu, L. M. Preparation of Rattle-type Magnetic Mesoporous Carbon Spheres and Their Highly Efficient Adsorption and Separation. *J. Colloid Interface Sci.* **2011**, *361*, 527−533.
(26) Yin, P.; Sun, N. R.; Deng, C. H.; Li, Y.; Zhang, X. M.; Yang, P. Y. Facile Preparation of Magnetic Graphene Double-Sided Mesoporous Composites for the Selective Enrichment and Analysis of Endogenous Peptides. *Proteomics* **2013**, *13*, 2243−2250.
(27) Zhao, M.; Deng, C. H.; Zhang, X. M. Synthesis of Polydopamine-Coated Magnetic Graphene for Cu^{2+} Immobilization and Application to the Enrichment of Low-Concentration Peptides for Mass Spectrometry Analysis. *ACS Appl. Mater. Interfaces* **2013**, *5*, 13104−13112.
(28) Du, X.; Wang, C. Y.; Chen, M. G.; Jiao, Y.; Wang, J. Electrochemical Performances of Nanoparticle Fe_3O_4/Activated Carbon Supercapacitor Using KOH Electrolyte Solution. *J. Phys. Chem. C* **2009**, *113*, 2643−2646.
(29) Dubal, D. P.; Lee, S. H.; Kim, J. G.; Kim, W. B.; Lokhande, C. D. Porous Polypyrrole Clusters Prepared by Electropolymerization for a High Performance Supercapacitor. *J. Mater. Chem.* **2012**, *22*, 3044−3052.
(30) Mu, J. B.; Chen, B.; Guo, Z. C.; Zhang, M. Y.; Zhang, Z. Y.; Zhang, P.; Shao, C. L.; Liu, Y. C. Highly Dispersed Fe_3O_4 Nanosheets on One-Dimensional Carbon Nanofibers: Synthesis, Formation Mechanism, and Electrochemical Performance as Supercapacitor Electrode Materials. *Nanoscale* **2011**, *3*, 5034−5040.
(31) You, L. J.; Xu, S.; Ma, W. F.; Li, D.; Zhang, Y. T.; Guo, J.; Hu, J. J.; Wang, C. C. Ultrafast Hydrothermal Synthesis of High Quality Magnetic Core Phenol−Formaldehyde Shell Composite Microspheres Using the Microwave Method. *Langmuir* **2012**, *28*, 10565−10572.
(32) Xu, S.; Ma, W. F.; You, L. J.; Li, J. M.; Guo, J.; Hu, J. J.; Wang, C. C. Toward Designer Magnetite/Polystyrene Colloidal Composite Microspheres with Controllable Nanostructures and Desirable Surface Functionalities. *Langmuir* **2012**, *28*, 3271−3278.
(33) Dai, X. Y.; Zhang, X.; Meng, Y. F.; Shen, P. K. Preparation of Hollow Carbon Spheres by Carbonization of Polystyrene/Polyaniline Core−Shell Polymer Particles. *New Carbon Mater.* **2011**, *26*, 389−395.
(34) Liu, N. L.; Qi, S. H.; Li, S. S.; Wu, X. M.; Wu, L. M. Preparation and Characterization of Phenol Formaldehyde/Ag/Graphite Nanosheet Composites. *Polym. Test.* **2011**, *30*, 390−396.
(35) Lu, A. H.; Sun, T.; Li, W. C.; Sun, Q.; Han, F.; Liu, D. H.; Guo, Y. Synthesis of Discrete and Dispersible Hollow Carbon Nanospheres with High Uniformity by Using Confined Nanospace Pyrolysis. *Angew. Chem., Int. Ed.* **2011**, *50*, 11765−11768.
(36) Zhang, L. L.; Zhao, X. S. Carbon-Based Materials as Supercapacitor Electrodes. *Chem. Soc. Rev.* **2009**, *38*, 2520−2531.
(37) Shen, W. W.; Xiong, H. M.; Xu, Y.; Cai, S. J.; Lu, H. J.; Yang, P. Y. ZnO−Poly(methyl methacrylate) Nanobeads for Enriching and Desalting Low-Abundant Proteins Followed by Directly MALDI-TOF MS Analysis. *Anal. Chem.* **2008**, *80*, 6758−6763.
(38) Lin, Y. H.; Wei, T. Y.; Chien, H. C.; Lu, S. Y. Manganese Oxide/Carbon Aerogel Composite: an Outstanding Supercapacitor Electrode Material. *Adv. Energy Mater.* **2011**, *1*, 901−907.
(39) Kim, Y. H.; Park, S. J. Roles of Nanosized Fe_3O_4 on Supercapacitive Properties of Carbon Nanotubes. *Curr. Appl. Phys.* **2011**, *11*, 462−466.
(40) Wang, D. W.; Li, Y. Q.; Wang, Q. H.; Wang, T. M. Nanostructured Fe_2O_3−Graphene Composite as a Novel Electrode Material for Supercapacitors. *J. Solid State Electrochem.* **2012**, *16*, 2095−2102.
(41) Mu, J. B.; Chen, B.; Guo, Z. C.; Zhang, M. Y.; Zhang, Z. Y.; Zhang, P.; Shao, C. L.; Liu, Y. C. Highly Dispersed Fe_3O_4 Nanosheets on One-Dimensional Carbon Nanofibers: Synthesis, Formation Mechanism, and Electrochemical Performance as Supercapacitor Electrode Materials. *Nanoscale* **2011**, *3*, 5034−5040.